JACS
JOURNAL OF THE AMERICAN CHEMICAL SOCIETY
Article
pubs.acs.org/JACS

Morphology Control of Nanofibril Donor–Acceptor Heterojunction To Achieve High Photoconductivity: Exploration of New Molecular Design Rule

Helin Huang,[†,§] Ching-En Chou,[‡,§] Yanke Che,[†] Ligui Li,[†] Chen Wang,[†] Xiaomei Yang,[†] Zhonghua Peng,*[,‡] and Ling Zang*[,†]

[†]Department of Materials Science and Engineering, University of Utah, 36 S. Wasatch Dr., Salt Lake City, Utah 84112, United States
[‡]Department of Chemistry, University of Missouri-Kansas City, Kansas City, Missouri 64110, United States

Supporting Information

ABSTRACT: Donor–acceptor nanofibril composites have been fabricated, and the dependence of their photocurrent response on the structure and morphology of the donor part has been systematically investigated. The nanofibril composites were composed of template nanofibers, assembled from an electron acceptor molecule, perylene tetracarboxylic diimide (PTCDI), onto which (through drop-casting) various electron donor molecules (**D1**–**D4**) were coated. The donor molecules have the same π-conjugated core, but different side groups. Due to the different side groups, the four donor molecules showed distinctly different propensity for intermolecular aggregation, with **D1**–**D3** forming segregated phases, while **D4** prefers homogeneous molecular distribution within the film. It was found that the nanofibril composites with **D4** exhibit the highest photocurrent, whereas those with aggregation-prone **D1**–**D3** exhibited much lower photocurrent under the same illumination condition. Solvent annealing is found to further enhance the aggregation of **D1**–**D3** but facilitate more uniform molecular distribution of **D4** molecules. As a result, the photocurrent response of PTCDI fibers coated with **D1**–**D3** decreased after vapor annealing, whereas those coated with **D4** further increased. The detrimental effect of the aggregation of donor molecules on the PTCDI fiber is likely due to the enhanced local electrical field built up by the high charge density around the aggregate–nanofiber interface, which hinders the charge separation of the photogenerated electron–hole pair. The results reported in this study give further insight into the molecular structural effect on photoconductivity of hybrid materials, particularly those based on donor–acceptor composites or interfaces, and provide new molecular design rules and material processing guidelines to achieve high photoconductivity.

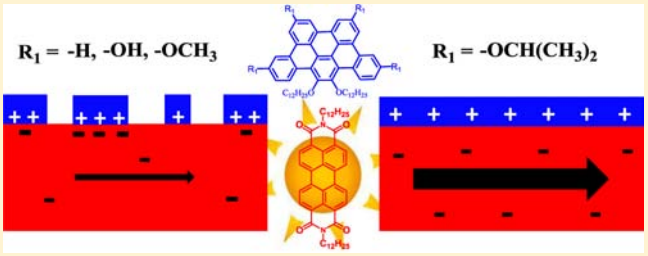

INTRODUCTION

Fabrication of effective donor–acceptor heterojunction structures remains critical for developing high-performance organic photovoltaics and the relevant photoelectric switches and sensors.[1−5] However, most of the research efforts to date have been focused on bulk heterojunctions, which are formed through the not-easily controlled phase separation process.[6−12] More ordered heterojunction structures, particularly those controllable at the nanometer scale through molecular design and engineering, are desirable in order to achieve high photoconversion efficiency.[13] Self-assembly has proven to be an efficient bottom-up method to construct well-defined nanostructures that may afford high photoconductivity.[14−16] A few examples have been reported on the design and fabrication of nanostructured heterojunction systems through molecular self-assembly.[3,17−24] Most of these systems, however, either form well-ordered structure only on a small area or require complicated molecular synthesis and thus are not suited for practical applications.

Recently, we have developed a novel approach based on nanofibril heterojunction to achieve high photoconductivity for organic materials.[3] The approach relies on interfacial structural modification of nanofibers fabricated from electron acceptor (A) molecules, onto which a layer of electron donor (D) molecules is coated. The A molecules are based on derivatives of perylene tetracarboxylic diimide (PTCDI), which represent a robust class of semiconductor materials with high thermal and photo stability.[25] The strong hydrophobic interdigitation between the long alkyl side chains of D and A molecules enables efficient charge transfer between the two under photoexcitation. Such nanofibril heterojunctions possess two prominent features that are critical for efficient photocurrent generation: one is that the nanofibers both create a wide D/A interface for increased charge separation and act as long-range transport pathway for photogenerated charge carriers toward the electrodes; the other is that the alkyl side chains employed

Received: July 16, 2013
Published: October 4, 2013

   dx.doi.org/10.1021/ja407024u | J. Am. Chem. Soc. 2013, 135, 16490–16496

not only enable effective surface adsorption of D molecules on the nanofibers for effective electron-transfer communication but also facilitate spatial separation the photogenerated charge carriers to prevent their recombination. The surface coating method thus developed represents a simple, adaptable method that will allow for further improvement of organic photoconductivity through molecular design and supramolecular engineering. In the present work, we aim to explore the effects of aggregation of D molecules on the photoconductivity of nanofibril heterojunctions. A series of D molecules with varying side-chain modifications were synthesized[26] and investigated for the different intermolecular arrangements caused by $\pi-\pi$ stacking in balance with steric hindrance of side chains. Interestingly, it was observed that the different molecular assemblies of D resulted in distinctive phase segregation between D and A (the nanofiber), which significantly affects the interfacial charge transfer and separation as indicated from the measurements of fluorescence quenching and photocurrent generation.

RESULTS AND DISCUSSION

Nanofibril Heterojunction Fabrication. Scheme 1 shows the structures of the four D molecules employed in this study,

Scheme 1. Schematic Illustration of Core-Shell Structured Nanofibril Heterojunction Composed of D1−D4 Coating and PTCDI Nanofiber

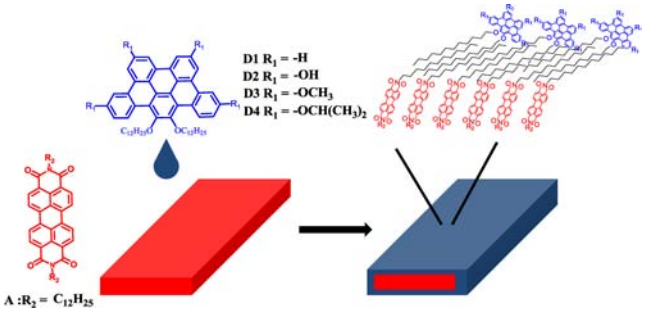

which are based on the same tribenzopentaphene (TBP) core. The rigid, planar π-conjugated TBP core is conducive for cofacial $\pi-\pi$ stacking that often leads to the formation of a one-dimensional molecular assembly. The highest occupied molecular orbital (HOMO) of TBP molecules is significantly higher than that of PTCDI, providing sufficient driving force for the photoinduced TBP to PTCDI electron transfer. All four TBP molecules (**D1−D4**) have two dodecyl chains attached at the same positions. These linear alkyl chains help anchoring the D molecules onto the nanofiber of A through hydrophobic alkyl chain interdigitation as observed before.[3,25,27] At the periphery of the TBP core, different side chains were attached for **D1−D4** so that the intermolecular arrangement between TBP cores can be modulated, whereas the interfacial interaction between PTCDI and the four D molecules is expected to be comparable due to their identical dodecyl anchoring chains. Systematic investigation on how the intermolecular aggregation of the coated D molecules affect the photocurrent response of the PTCDI nanofibers would provide deeper understanding of the photoinduced charge separation process at the nanofibril heterojunction and open more options to further increase the photocurrent through structural optimization of the D component.

Side group modification has proven to be an effective way for tuning the intermolecular interactions, leading to different aggregated morphologies and electronic properties.[28] Such molecular structural effect can be more clearly manifested under solvent vapor annealing, which facilitates the self-assembly of molecules to reach the thermodynamically stable (energy minimal) state by removing the grain boundaries formed during the fast solvent vaporization process. Indeed, solvent vapor annealing has been extensively studied for organic semiconductor materials and devices in order to improve the crystallinity and charge carrier mobility.[29−32] In this study, we adopted this annealing process to facilitate the assembly of D molecules so that the effect of peripheral side group modification can be revealed more illustriously. Among the four D molecules, **D4** is expected to have the most severe steric hindrance for $\pi-\pi$ stacking due to its bulkier side groups. The other three molecules on the other hand possess relatively small peripheral groups and are thus prone to $\pi-\pi$ staking aggregation. As shown below, the different extent of intermolecular aggregation in the four D molecules has a dramatic effect on the photocurrent response of the core PTCDI nanofibers. With the coating of **D4**, which shows no $\pi-\pi$ stacking even after solvent annealing, the PTCDI nanofibers exhibit the highest photocurrent. When coated with **D1**, **D2**, and **D3** molecules, which are prone to aggregation, the photocurrent response is significantly lower. The difference is more dramatic for the D−A nanofibril heterojunctions after solvent vapor annealing.

The nanofiber of A was fabricated from a PTCDI molecule (Scheme 1) following the previously published self-assembly protocol.[27] The PTCDI molecule has a dodecyl chain at both imide positions to ensure strong hydrophobic alkyl chain interdigitation with the D molecules. The nanofibers were subsequently surface-coated with D molecules using the drop casting method previously employed for creating similar nanofibril heterojunctions.[3] The as-prepared nanofibers possess well-defined morphologies and large aspect ratios, providing a large interface for surface adsorption of D molecules. Figure 1

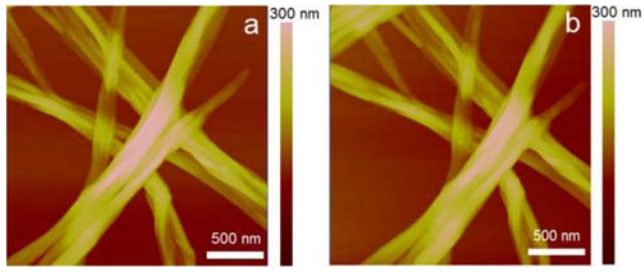

Figure 1. AFM images of PTCDI nanofibers (molecular amount of 7 nmol) deposited on a 5 mm × 5 mm silicon wafer covered with 300-nm thick SiO_2 before (a) and after (b) surface coating of **D4** (4 nmol).

shows the in situ AFM images of PTCDI nanofibers before and after surface coating of **D4** molecules. Almost all of the D molecules are coated onto the surface of nanofibers after drop casting, leaving little residue on the silicon oxide substrate. Similar phenomena were observed for other three D molecules, **D1−D3** (Supplementary Figure S1). The clean and selective deposit of D molecules onto the PTCDI fibers is attributed to the strong hydrophobic interdigitation between the dodecyl chains of D and that of PTCDI molecules on the nanofiber surface. Meanwhile, the morphology of individual nanofibers

dx.doi.org/10.1021/ja407024u | J. Am. Chem. Soc. 2013, 135, 16490−16496

and the intertwining configuration remain unchanged after drop casting, indicating the robustness of nanofibril structures on the substrate. Such a feature enables comparative studies of PTCDI nanofibers modified with different D molecules, allowing the pinpointing of different photocurrent responses on the surface-coated D molecules.

Effect of Intermolecular Aggregation Photoconductivity. Figure 2a shows the fluorescence spectra of the PTCDI

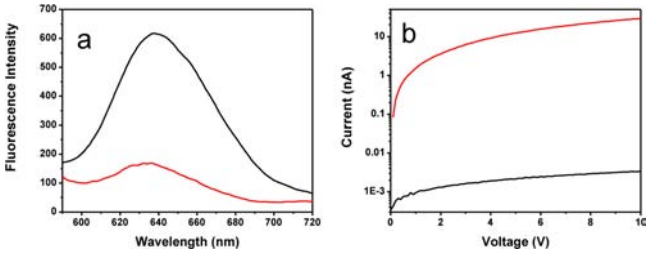

Figure 2. (a) Fluorescence spectra of PTCDI nanofibers shown in Figure 1 before (black) and after (red) drop-casting of **D4**. (b) I–V curves measured over the **D4**-coated PTCDI nanofibers in the dark (black) and under white light irradiation of 0.17 mW/mm^2 (red). Efficient fluorescence quenching of PTCDI nanofibers by coating of **D4** was also confirmed with fluorescence microscopy imaging (Supplementary Figure S12). Similar fluorescence quenching was also observed for the coating of **D1**–**D3** molecules (Supplementary Figures S5 and S13).

nanofibers before and after the coating of **D4** molecules, which indicates that 80% of the PTCDI fluorescence was quenched after **D4** coating. The significant fluorescence quenching is due to the forward electron transfer from **D4** molecules to the photoexcited PTCDIs. This photoinduced electron transfer is thermodynamically favored with a driving force of 1.13 eV, calculated between the highest occupied molecular orbital (HOMO) levels of **D4** and PTCDI molecules (Figure 3). Consistent with the efficient fluorescence quenching, high photoconductivity was observed for the **D4**/PTCDI nanofibril heterojunction (Figure 2b), for which an on/off ratio of ca. 10^4 was obtained under a 10 V bias. The high photoconductivity was due to an optimal balance between the forward and back electron transfer between **D4** coating and the PTCDI nanofibers as discussed below. It is possible that the increased photocurrent may be due to the conductivity of the **D4** coating itself. However, this possibility was excluded since the dark and photo current of **D4** film under the same light illumination (Supplementary Figure S7) was only around 1 pA under 10 V bias, which is 3 orders of magnitude lower than that of **D4**/PTCDI nanofibers (Figure 2b). Moreover, the **D4** film does not demonstrate photoconductivity response, i.e., the I–V curves obtained under dark and light illumination remained almost the same (Supplementary Figure S7).

The same experiments shown in Figure 2 were also performed on the PTCDI nanofibers coated with other three D molecules, **D1**–**D3**, in order to investigate the effect of molecular structure of D on the photoconductivity of D/A nanofibril heterojunctions. Figure 3 shows the results of fluorescence quenching and photocurrent measurements performed on the four different nanofibril heterojunctions. While all four nanofibers showed comparable fluorescence quenching after D-coating, the photocurrents generated were dramatically different, with the **D4**/PTCDI nanofiber giving the highest photocurrent. The efficient fluorescence quenching is

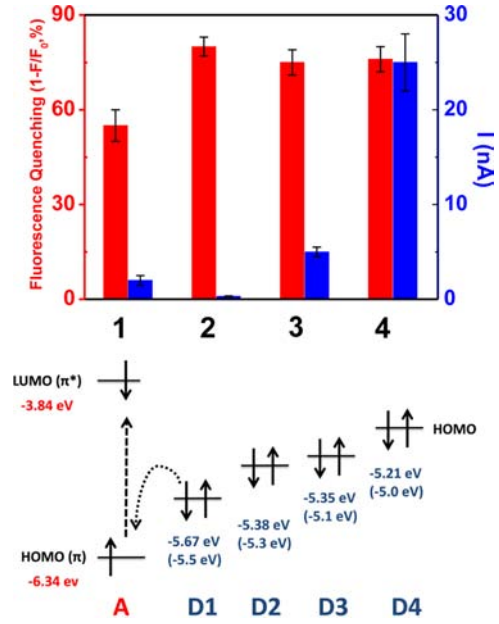

Figure 3. (Top) Comparison of fluorescence quenching (red) and photocurrent generation (blue) between the PTCDI nanofibers coated with the four donor molecules, **D1**–**D4**. Fluorescence quenching and photocurrent measurements were conducted under the same conditions as employed in Figure 2. Photocurrent values used in this plot were obtained at a bias voltage of 10 V. Example fluorescence quenching and I–V curves measured over **D1**–**D4** are shown in Figure 2 and Supplementary Figures S5 and S6. (Bottom) Electronic energy levels of PTCDI and **D1**–**D4**. The HOMO levels of **D1**–**D4** were determined by cyclic voltammetry using Fc/Fc$^+$ as an internal standard.[26] The energy levels of PTCDI (A) and **D1**–**D4** (in parentheses) were calculated with density-functional theory (B3LYP/6-311g**//B3LYP/6-31g*) using the Gaussian 09 package.

consistent with the energetically favorable forward electron transfer from the D molecule to the photoexcited A, for which the driving force was calculated to be in the range of 0.7–1.1 eV (Figure 3). However, efficient forward electron transfer does not necessarily produce high electrical current, which also depends on other factors such as the subsequent charge separation of the photogenerated D$^+$–A$^-$ pair to free charge carriers and the charge carrier mobility. Charge recombination (or back electron transfer) within D$^+$–A$^-$ pair is often one of the major reasons for low photocurrent.

It is particularly intriguing to compare **D3** and **D4**. Both have alkoxy side groups and very close HOMO levels. When coated on PTCDI fibers, they exhibit an identical extent of fluorescence quenching. The photocurrent response of the two heterojunctions, however, differs by almost five times. The difference in photocurrent was even more dramatic for the nanofibers coated with **D1** and **D2**, which showed photocurrent values more than 10 and 50 times, respectively lower than that of **D4**-coated fibers (Figure 3). Considering the similar fluorescence quenching efficiency among the four nanofibers, we suspected that the lower photocurrent observed with the nanofibers coated with **D1**–**D3** (compared to that of **D4**) was primarily due to the less efficient charge separation (or faster charge recombination) of the photogenerated D$^+$–A$^-$ pair, which has something to do with the phase segregation of surface-coated D molecules. The bulky side group of **D4** prevents intermolecular π–π stacking, resulting in uniform molecular distribution of **D4** onto the PTCDI nanofibers. In

dx.doi.org/10.1021/ja407024u | J. Am. Chem. Soc. 2013, 135, 16490–16496

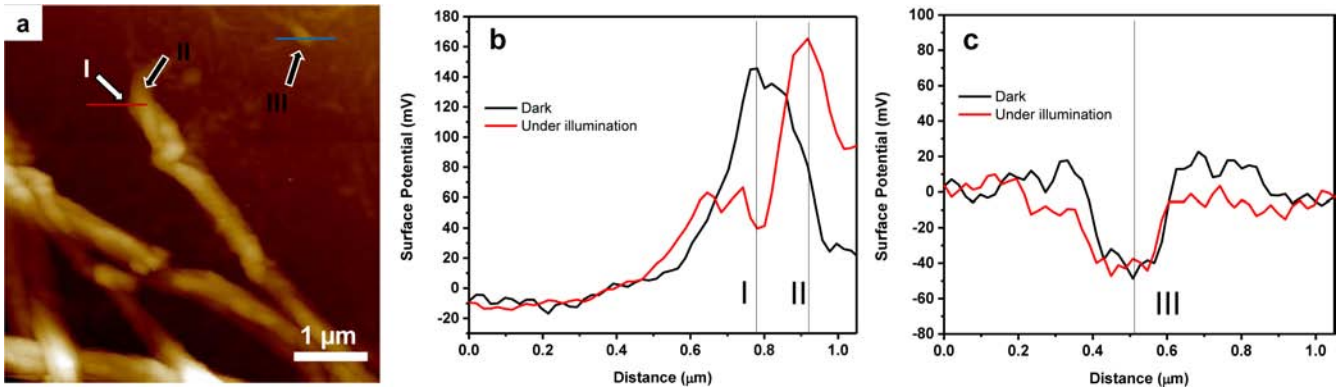

Figure 4. KPFM measurement of **D3**/PTCDI nanofibril heterojunction. (a) Topograhy image of the nanofibril heterojunction (*Z* height range 400 nm). PTCDI nanofiber, **D3** coating, and isolated **D3** aggregate are marked as domains I, II, and III, respectively. (b, c) Line scan surface potential profiles obtained by tracing the corresponding lines marked (red, blue) in the dark (black plot) and under white light illumination of 10 mW/cm^2 (red plot).

contrast, **D1**−**D3**, with relatively small side groups, are prone to π−π stacking, which leads to the formation of segregated phases of aggregated D molecules. AFM images of the drop-cast films of **D1**−**D3** confirmed their self-assembly. Particularly for **D1** and **D3**, the preferred columnar stacking enabled formation of nanofibril structures (Supplementary Figures S2 and S10).

Results in Figure 3 suggest that aggregates of **D1**−**D3** can quench the fluorescence of PTCDI nanofiber in similar (or comparable) efficiency as the homogeneous coating of **D4**. This can be explained by the long distance exciton migration within the single crystalline nanofiber of PTCDI, where the exciton migration distance was in the range of hundreds of nanometers.[25,33] Once the quenchers (molecules or aggregates) are distributed on the surface with sufficient density (i.e., spatially separated within the distance of exciton migration), the fluorescence of nanofibers can be effectively quenched, as an exciton can always encounter a quencher when migrating along the nanofiber within its lifetime.[34] Considering the high molar ratio (4/7) of D/A used in this study, it is reasonable to assume that the aggregates of **D1**−**D3** can cover the PTCDI nanofiber with high enough density and the separation between the aggregates is significantly smaller than the exciton migration distance of PTCDI.

Although the aggregation of **D1**−**D3** does not affect fluorescence quenching efficiency, it caused significant decrease in photocurrent compared to the case of **D4**. This is likely due to the locally enhanced recombination (rather than separation) of the D^+−A^- charge pair photogenerated around the aggregate of D. The interfacial charge separation of D^+−A^- at the PTCDI nanofiber is primarily caused by the intermolecular electron delocalization among the π−π stacked PTCDI molecules,[3,5,35] and this charge delocalization can be further extended under electrical bias applied to the nanofiber. At the fibril section with an aggregated D domain, there may be multiple pairs of D^+−A^- photogenerated by quenching multiple excitons (as discussed above), making the electron delocalization along the PTCDI stacks more difficult due to the increased charge density.[36,37] Moreover, multiple charge pairs form a strong local electrical field, which can prevent the charge separation. These two effects result in enhanced charge recombination of D^+−A^-. In contrast, the homogeneous coating of **D4** produces more uniform distribution of D^+−A^- pairs on the nanofiber, which can be effectively separated through the intermolecular electron delocalization along the nanofiber, leading to the generation of high photocurrent as shown in Figure 3.

It is interesting to note that among the three D molecules (**D1**−**D3**) that produced relatively low photocurrent (Figure 3), **D2** demonstrated the lowest current value, significantly lower than the other two, although the fluorescence quenching efficiency of **D2** is even the highest. This additional lowering of photoconductivity is likely due to the hydroxyl side groups of **D2** (−OH), which affords redox interaction with electrons, functioning as a charge carrier trap as previously observed in n-type organic field effect transistors.[38−40]

Surface Potential of Nanofibril Heterojunction under Illumination. To gain further insight into the photoinduced charge separation process within the nanofibril heterojunction of PTCDI, Kelvin probe force microscopy (KPFM) was used to image the surface potential change upon illumination in a similar way as previously performed on other organic heterojunctions.[41,42] **D3** was chosen as a representative of the three donors (**D1**−**D3**) to form D/A heterojunction with PTCDI; these three donors prefer to form aggregates, which are easy to be imaged by AFM and distinguished from PTCDI fiber. The **D3**/PTCDI nanofibers were deposited onto an indium-doped tin oxide (ITO) coated glass slide, and measured simultaneously for topography and surface potential images both in the dark and under white light illumination.

As shown in Figure 4a, well-defined morphology was observed for the PTCDI nanofiber with surface coating of **D3**. Figure 4b shows the line scan profile of surface potential corresponding to the red line marked in Figure 4a. In the dark, the surface potential PTCDI fiber (domain I as marked) appears higher than that of **D3** aggregate (domain II), consistent with their HOMO level difference as shown in Figure 3. Upon white light illumination, PTCDI gets excited, initiating electron transfer from **D3** to the fiber. This charge separation was imaged as an increase in surface potential of the **D3** phase, but a decrease for the PTCDI fiber (red plot in Figure 4b). For comparison, the same KPFM measurements were also performed on a bare **D3** aggregate (domain III), for which no surface potential change was observed before and after white illumination (Figure 4c). This is simply because that **D3** can barely be excited by visible light (Figure S3) and thus no charge separation can be initiated.

Solvent-Annealing Influence on Photoconductivity. It is well-known that fast evaporation of solvents during the drop-

dx.doi.org/10.1021/ja407024u | J. Am. Chem. Soc. 2013, 135, 16490−16496

casting process rarely produces the thermodynamically stable (energy minimized) state with regard to the intermolecular arrangement and phase growth within organic materials. Large number of defects and grain boundaries can be formed during the rapid assembly of molecules, and the growth of small nuclei may be quenched when the solvent is dried. Postassembly treatment, like solvent vapor annealing (i.e., aging of organic materials in saturated solvent vapor), has proven to be an effective method to reorganize and optimize the intermolecular arrangement, and facilitate the phase growth to reach the thermodynamic stable state.[29,43−46] Indeed, solvent vapor annealing has been commonly used in solar cell materials processing to improve the crystalline organization of D and A phases, with the aim to facilitate the charge transportation.[9,47−53] We expected that the above-mentioned difference of photocurrent between the nanofibers coated with **D4** and **D1**−**D3** would be more profound if the nanofibers were subject to solvent vapor annealing, considering that the difference of phase morphology and its dependence on the molecular structure between **D4** and **D1**−**D3** can be maximized at the thermodynamic stable state.

D3 was chosen as a representative of **D1**−**D3** to study the effects of solvent vapor annealing on the surface aggregation and the subsequent photoconductivity; the results were compared to those observed with **D4**. The annealing was performed in ethanol vapor, as ethanol is a good solvent for **D1**−**D4**, but a poor one for the PTCDI. During the annealing process the crystalline structure of PTCDI nanofibers was expected to remain intact. Under the same annealing conditions, **D3** and **D4** coatings underwent dramatically different transition of the aggregation state. For **D3**, optical microscopy imaging showed the growth of small aggregates into large needle like structures (Figure S10). AFM imaging revealed that the small aggregates of **D3** are actually composed of fine nanofibril structures, which were formed during the drop-cast process. Formation of nanofibril structure is indicative of the favorable columnar $\pi-\pi$ stacking of **D3**, which is consistent with planar geometry of TBP π-conjugation. Upon solvent vapor annealing these small nanofibers grew into needle like chunks, though still remaining in an elongated shape (Figure S10). This observation indicates that **D3** is prone to crystallize into large elongated structures driven by the strong $\pi-\pi$ stacking interaction. The **D4** coating on the other hand showed no obvious aggregation even after solvent vapor annealing (Figure S11).

The different behavior of **D3** and **D4** under solvent vapor annealing led to distinct effect on the photocurrent response as measured over the PTCDI nanofibers coated with these two molecules (Figure 5a). For **D3**, the photocurrent decreased to 14% of its preannealing value, whereas for **D4**, the photocurrent increased by 60%. The significant decrease in photoconductivity of **D3**/PTCDI nanofiber is likely due to the increased aggregation of **D3** induced by the solvent vapor annealing. As discussed above, the enlarged aggregated domains of D molecules are detrimental to the charge separation of D^+-A^- pairs due to the enhanced local electrical field. In contrast, for the **D4**/PTCDI nanofiber the bulky isopropoxyl substitution at **D4** prevents molecular aggregation and instead favors the homogeneous distribution of molecules on the surface. Such molecular distribution can be further facilitated under solvent vapor annealing, producing a coating layer with minimized aggregation, as indicated by the 60% increase in photocurrent shown in Figure 5. This annealing-enhanced molecular

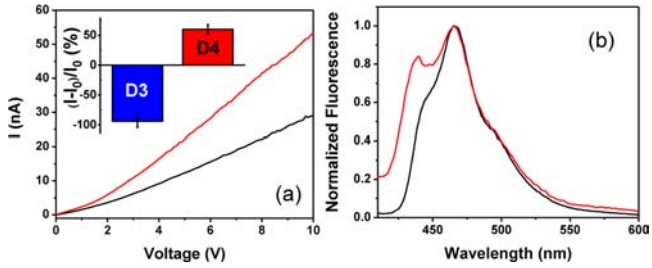

Figure 5. (a) I−V curves measured over **D4**-coated PTCDI nanofibers under the same light irradiation as employed in Figure 2 before (black) and after (red) solvent vapor annealing. Inset: relative photocurrent change (in percentage) for **D3**- and **D4**-coated nanofibers after solvent vapor annealing. Photocurrent values used in this plot were obtained at a bias voltage of 10 V. Example I−V curves for **D3**- and **D4**-coated nanofibers are shown in Supplementary Figure S8. (b) Fluorescence spectra of **D4** drop-cast on a glass surface modified with trichloro(octadecyl)silane (OTS) before (black) and after (red) solvent vapor annealing. The two spectra are normalized at 465 nm.

distribution of **D4** was supported by the solid-state fluorescence spectral measurement on a thin **D4** film drop-cast on a glass slide. The glass slide was pretreated with trichloro(octadecyl)-silane (OTS) to generate a hydrophobic surface similar to that of the PTCDI nanofiber. Before solvent vapor annealing, the fluorescence spectrum of **D4** film possesses a major peak at 465 nm, along with a shoulder peak at a shorter wavelength, 440 nm. Compared to the fluorescence spectrum of **D4** molecularly dispersed in ethanol (Supplementary Figure S3), the fluorescence emission in the solid state becomes more dominant at longer wavelength (Figure 5b), consistent with the enhanced intermolecular interaction as commonly observed for molecular assemblies. The 440 nm emission (characteristic of the fluorescence of individual molecules) remains in the solid film of **D4**, indicating the relatively weak intermolecular $\pi-\pi$ interaction in comparison with the film of **D3**, where the strong $\pi-\pi$ stacking results in almost no emission observed for the individual molecules (Supplementary Figures S3 and S4). After solvent vapor annealing, the 440 nm peak of **D4** film was significantly enhanced (Figure 5b), implying more molecules originally "frozen" as aggregates during the fast evaporation of drop-casting now transformed into homogeneous molecular distribution. In contrast, for the **D3** film there was no obvious change observed in the fluorescence spectrum upon solvent vapor annealing under the same condition (Supplementary Figure S9). This is consistent with the strong intermolecular stacking, which leads to the formation of stable aggregates in the specific nanofibril morphology (Supplementary Figure S10). Although solvent vapor annealing facilitates the growth of the nanofibers of **D3** into larger elongated crystals, the electronic property of the solid phase still remains dominant with the $\pi-\pi$ stacking as indicated by the unchanged fluorescence spectra.

CONCLUSIONS

In summary, we have investigated a series of electron donor molecules (**D1**−**D4**) that share the same π-conjugation core, but which are modified with different side groups. PTCDI fibers coated with such donor molecules showed dramatically different photocurrent response. It was found that the nanofibers coated with homogeneously and molecularly distributed donor molecules (such as **D4**) exhibit the highest photocurrent, whereas those coated with segregated donor

dx.doi.org/10.1021/ja407024u | J. Am. Chem. Soc. 2013, 135, 16490−16496

aggregates (such as **D1**−**D3**) show much lower photocurrent under the same illumination conditions. The aggregation of donor molecules on the surface of the PTCDI fibers may lead to the buildup of a local electrical field that hinders the charge separation of the photogenerated electron−hole pairs. The different morphologies of molecular aggregates were mostly the result of side group modification of the donor molecules. Such structural effect was more clearly manifested by investigating the structure and morphology change of the drop-cast films upon solvent vapor annealing. The findings presented provide new insight into the molecular structural effect on photoconductivity of organic semiconductor materials, particularly those based on donor−acceptor composites or interfaces, and open alternative ways to improve the photoconductivity by structural design and modification.

■ ASSOCIATED CONTENT

Supporting Information

Experimental methods and materials, additional spectral measurements, optical microscopy and AFM images. This material is available free of charge via the Internet at http://pubs.acs.org.

■ AUTHOR INFORMATION

Corresponding Authors

pengz@umkc.edu
lzang@eng.utah.edu

Author Contributions

[§]These authors contributed equally to this work.

Notes

The authors declare no competing financial interest.

■ ACKNOWLEDGMENTS

This work was supported by DHS (2009-ST-108-LR0005) and NSF (CHE 0931466). Z.P. acknowledges the support of NSF (DMR1308577) and the Army Research Office (W911NF-10-1-0476).

■ REFERENCES

(1) Günes, S.; Neugebauer, H.; Sariciftci, N. S. *Chem. Rev.* **2007**, *107*, 1324−1338.
(2) Thompson, B. C.; Fréchet, J. M. J. *Angew. Chem., Int. Ed.* **2008**, *47*, 58−77.
(3) Che, Y.; Huang, H.; Xu, M.; Zhang, C.; Bunes, B. R.; Yang, X.; Zang, L. *J. Am. Chem. Soc.* **2011**, *133*, 1087−1091.
(4) Konstantatos, G.; Sargent, E. H. *Nat. Nanotechnol.* **2010**, *5*, 391−400.
(5) Che, Y.; Yang, X.; Liu, G.; Yu, C.; Ji, H.; Zuo, J.; Zhao, J.; Zang, L. *J. Am. Chem. Soc.* **2010**, *132*, 5743−5750.
(6) Halls, J. J. M.; Walsh, C. A.; Greenham, N. C.; Marseglia, E. A.; Friend, R. H.; Moratti, S. C.; Holmes, A. B. *Nature* **1995**, *376*, 498−500.
(7) Yu, G.; Gao, J.; Hummelen, J. C.; Wudl, F.; Heeger, A. J. *Science* **1995**, *270*, 1789−1791.
(8) Peumans, P.; Uchida, S.; Forrest, S. R. *Nature* **2003**, *425*, 158−162.
(9) Li, G.; Shrotriya, V.; Huang, J.; Yao, Y.; Moriarty, T.; Emery, K.; Yang, Y. *Nat. Mater.* **2005**, *4*, 864−868.
(10) Kim, J. Y.; Lee, K.; Coates, N. E.; Moses, D.; Nguyen, T.-Q.; Dante, M.; Heeger, A. J. *Science* **2007**, *317*, 222−225.
(11) Park, S. H.; Roy, A.; Beaupre, S.; Cho, S.; Coates, N.; Moon, J. S.; Moses, D.; Leclerc, M.; Lee, K.; Heeger, A. J. *Nat. Photonics* **2009**, *3*, 297−302.
(12) He, Z.; Zhong, C.; Huang, X.; Wong, W.-Y.; Wu, H.; Chen, L.; Su, S.; Cao, Y. *Adv. Mater.* **2011**, *23*, 4636−4643.
(13) Chang, C.-Y.; Wu, C.-E.; Chen, S.-Y.; Cui, C.; Cheng, Y.-J.; Hsu, C.-S.; Wang, Y.-L.; Li, Y. *Angew. Chem., Int. Ed.* **2011**, *50*, 9386−9390.
(14) Hoeben, F. J. M.; Jonkheijm, P.; Meijer, E. W.; Schenning, A. P. H. J. *Chem. Rev.* **2005**, *105*, 1491−1546.
(15) De Greef, T. F. A.; Smulders, M. M. J.; Wolffs, M.; Schenning, A. P. H. J.; Sijbesma, R. P.; Meijer, E. W. *Chem. Rev.* **2009**, *109*, 5687−5754.
(16) Aida, T.; Meijer, E. W.; Stupp, S. I. *Science* **2012**, *335*, 813−817.
(17) Percec, V.; Glodde, M.; Bera, T. K.; Miura, Y.; Shiyanovskaya, I.; Singer, K. D.; Balagurusamy, V. S. K.; Heiney, P. A.; Schnell, I.; Rapp, A.; Spiess, H. W.; Hudson, S. D.; Duan, H. *Nature* **2002**, *417*, 384−387.
(18) Würthner, F.; Chen, Z.; Hoeben, F. J. M.; Osswald, P.; You, C.-C.; Jonkheijm, P.; Herrikhuyzen, J. v.; Schenning, A. P. H. J.; van der Schoot, P. P. A. M.; Meijer, E. W.; Beckers, E. H. A.; Meskers, S. C. J.; Janssen, R. A. J. *J. Am. Chem. Soc.* **2004**, *126*, 10611−10618.
(19) Yamamoto, Y.; Fukushima, T.; Suna, Y.; Ishii, N.; Saeki, A.; Seki, S.; Tagawa, S.; Taniguchi, M.; Kawai, T.; Aida, T. *Science* **2006**, *314*, 1761−1764.
(20) Sisson, A. L.; Sakai, N.; Banerji, N.; Fürstenberg, A.; Vauthey, E.; Matile, S. *Angew. Chem., Int. Ed.* **2008**, *47*, 3727−3729.
(21) Yamamoto, Y.; Zhang, G.; Jin, W.; Fukushima, T.; Ishii, N.; Saeki, A.; Seki, S.; Tagawa, S.; Minari, T.; Tsukagoshi, K.; Aida, T. *Proc. Natl. Acad. Sci. U.S.A.* **2009**, *106*, 21051−21056.
(22) Sakai, N.; Bhosale, R.; Emery, D.; Mareda, J.; Matile, S. *J. Am. Chem. Soc.* **2010**, *132*, 6923−6925.
(23) Zhang, W.; Jin, W.; Fukushima, T.; Saeki, A.; Seki, S.; Aida, T. *Science* **2011**, *334*, 340−343.
(24) Sakai, N.; Matile, S. *J. Am. Chem. Soc.* **2011**, *133*, 18542−18545.
(25) Zang, L.; Che, Y.; Moore, J. S. *Acc. Chem. Res.* **2008**, *41*, 1596−1608.
(26) Chou, C.-E.; Li, Y.; Che, Y.; Zang, L.; Peng, Z. *RSC Adv.* **2013**, *3*, 20666−20672.
(27) Balakrishnan, K.; Datar, A.; Naddo, T.; Huang, J.; Oitker, R.; Yen, M.; Zhao, J.; Zang, L. *J. Am. Chem. Soc.* **2006**, *128*, 7390−7398.
(28) Nguyen, L. H.; Hoppe, H.; Erb, T.; Günes, S.; Gobsch, G.; Sariciftci, N. S. *Adv. Funct. Mater.* **2007**, *17*, 1071−1078.
(29) Datar, A.; Oitker, R.; Zang, L. *Chem. Commun.* **2006**, 1649−1651.
(30) Dickey, K. C.; Anthony, J. E.; Loo, Y. L. *Adv. Mater.* **2006**, *18*, 1721−1726.
(31) Lu, G.; Li, L.; Yang, X. *Small* **2008**, *4*, 601−606.
(32) Chen, H.; Hu, S.; Zang, H.; Hu, B.; Dadmun, M. *Adv. Funct. Mater.* **2013**, *23*, 1701−1710.
(33) Chaudhuri, D.; Li, D.; Che, Y.; Shafran, E.; Gerton, J. M.; Zang, L.; Lupton, J. M. *Nano Lett.* **2011**, *11*, 488−492.
(34) Naddo, T.; Che, Y.; Zhang, W.; Balakrishnan, K.; Yang, X.; Yen, M.; Zhao, J.; Moore, J. S.; Zang, L. *J. Am. Chem. Soc.* **2007**, *129*, 6978−6979.
(35) Che, Y.; Datar, A.; Yang, X.; Naddo, T.; Zhao, J.; Zang, L. *J. Am. Chem. Soc.* **2007**, *129*, 6354−6355.
(36) Delgado, M. C. R.; Kim, E.-G.; Filho, D. t. A. d. S.; Bredas, J.-L. *J. Am. Chem. Soc.* **2010**, *132*, 3375−3387.
(37) Coropceanu, V.; Cornil, J.; da Silva Filho, D. A.; Olivier, Y.; Silbey, R.; Brédas, J.-L. *Chem. Rev.* **2007**, *107*, 926−952.
(38) Chua, L.-L.; Zaumseil, J.; Chang, J.-F.; Ou, E. C. W.; Ho, P. K. H.; Sirringhaus, H.; Friend, R. H. *Nature* **2005**, *434*, 194−199.
(39) Yoon, M.-H.; Kim, C.; Facchetti, A.; Marks, T. J. *J. Am. Chem. Soc.* **2006**, *128*, 12851−12869.
(40) Baeg, K.-J.; Facchetti, A.; Noh, Y.-Y. *J. Mater. Chem.* **2012**, *22*, 21138−21143.
(41) Liscio, A.; De Luca, G.; Nolde, F.; Palermo, V.; Müllen, K.; Samorì, P. *J. Am. Chem. Soc.* **2008**, *130*, 780−781.
(42) Palermo, V.; Otten, M. B. J.; Liscio, A.; Schwartz, E.; de Witte, P. A. J.; Castriciano, M. A.; Wienk, M. M.; Nolde, F.; De Luca, G.; Cornelissen, J. J. L. M.; Janssen, R. A. J.; Müllen, K.; Rowan, A. E.; Nolte, R. J. M.; Samorì, P. *J. Am. Chem. Soc.* **2008**, *130*, 14605−14614.

(43) Campoy-Quiles, M.; Ferenczi, T.; Agostinelli, T.; Etchegoin, P. G.; Kim, Y.; Anthopoulos, T. D.; Stavrinou, P. N.; Bradley, D. D. C.; Nelson, J. *Nat. Mater.* **2008**, *7*, 158−164.
(44) De Luca, G.; Liscio, A.; Battagliarin, G.; Chen, L.; Scolaro, L. M.; Müllen, K.; Samorì, P.; Palermo, V. *Chem. Commun.* **2013**, *49*, 4322−4324.
(45) De Luca, G.; Liscio, A.; Maccagnani, P.; Nolde, F.; Palermo, V.; Müllen, K.; Samorì, P. *Adv. Funct. Mater.* **2007**, *17*, 3791−3798.
(46) De Luca, G.; Liscio, A.; Nolde, F.; Scolaro, L. M.; Palermo, V.; Müllen, K.; Samorì, P. *Soft Matter* **2008**, *4*, 2064−2070.
(47) Hoppe, H.; Sariciftci, N. S. *J. Mater. Chem.* **2006**, *16*, 45−61.
(48) Yang, X.; Loos, J.; Veenstra, S. C.; Verhees, W. J. H.; Wienk, M. M.; Kroon, J. M.; Michels, M. A. J.; Janssen, R. A. J. *Nano Lett.* **2005**, *5*, 579−583.
(49) Kim, H. J.; Lee, H. H.; Kim, J.-J. *Macromol. Rapid Commun.* **2009**, *30*, 1269−1273.
(50) Zhao, Y.; Xie, Z.; Qu, Y.; Geng, Y.; Wang, L. *Appl. Phys. Lett.* **2007**, *90*, 043504.
(51) Jo, J.; Na, S.-I.; Kim, S.-S.; Lee, T.-W.; Chung, Y.; Kang, S.-J.; Vak, D.; Kim, D.-Y. *Adv. Funct. Mater.* **2009**, *19*, 2398−2406.
(52) Bavel, S. S. v.; Sourty, E.; With, G. d.; Loos, J. *Nano Lett.* **2008**, *9*, 507−513.
(53) Li, G.; Yao, Y.; Yang, H.; Shrotriya, V.; Yang, G.; Yang, Y. *Adv. Funct. Mater.* **2007**, *17*, 1636−1644.